frontiers

The role of spatiotemporal correlations in the encoding and retrieval of synaptic patterns by STDP in recurrent spiking networks

Quan Zou [1,*], **Philip H. Goodman** [2] **and Frederick C. Harris, Jr.** [3]

[1] *Department of Statistics, The George Washington University, Washington, DC 20052, USA*
[2] *School of Medicine and Program in Biomedical Engineering, University of Nevada, Reno, NV 89557, USA*
[3] *Department of Computer Science and Engineering, University of Nevada, Reno, NV 89557, USA*

Correspondence*:
Quan Zou
my current address, qzou@gwu.edu

ABSTRACT

Spike-timing dependent plasticity (STDP) is considered to be an important synaptic mechanism to encode information within and between cerebral cortical networks. It remains unclear, however, how temporal and spatial correlations of signals and ongoing background spiking activity interact with STDP mechanisms to give rise to long-term memory. Because cortical networks mostly contain local recurrent connections, it is critical to explore STDP-based encoding and decoding of synaptic patterns in such architectures. In order to investigate their dynamics, we applied a phenomenological STDP model within recurrent networks, and between recurrent and feed-forward networks. We find that emergence of transient spatiotemporal correlations of ongoing activity lead to the storage of self-organized, simple synaptic patterns in the recurrent networks. These networks can be probed at a later time to reconstruct the encoded patterns by projecting them onto another network in a feed-forward, readout fashion with highly correlated spatiotemporal structure. We hypothesize that transient spatiotemporal correlations among networks can serve as a biologically plausible mechanism of memory storage and retrieval based on STDP.

Keywords: spike-timing dependent plasticity, spatiotemporal correlation, recurrent network, synaptic pattern, memory encoding and retrieval

1 INTRODUCTION

The theoretical dependence of excitatory synaptic efficacy upon the relative timing of pre-synaptic and post-synaptic action potentials, also referred to as spike-timing dependent plasticity (STDP), has been experimentally confirmed (Markram et al. (1997); Bi and Poo (1998); Bell et al. (1997); Magee and Johnston (1997)). Potentiation is typically observed when the excitatory post-synaptic potential (EPSP) precedes the post-synaptic spike, whereas the reversed temporal order induces depression of the synaptic transmission. A great number of computational models have been proposed to account for the dynamics of STDP (see review in Morrison et al. (2007)). They can be categorized into two basic types: “hard-bound”

models, in which synaptic weights are maintained between minimal and maximal values (Song et al. (2000)), and "soft-bound" models, in which synaptic weights progressively saturate to equilibrium (Kistler and van Hemmen (2000); van Rossum et al. (2000); Badoual et al. (2006); Morrison et al. (2007); Zou and Destexhe (2007)). These models have been used, for example, to explain cortical remapping during development (Song and Abbott (2001)) and cross-model coordinate transformation (Davison and Frégnac (2006)).

Recurrent networks, comprised of "internal" links, connecting neurons to one another in an undirected manner, may generate their own internal dynamic representations when subjected to external stimuli. To perform computation in recurrent networks, STDP can be used as the mechanism modifying connection strengths across all synapses. Kitano et al. (2002), demonstrated that STDP, when applied to a self-organized recurrent network, can result in asynchronous activity at 20∼30 Hz, during delay periods of working memory task. It also has been claimed that STDP can initiate resonant or rhythmic activity dominated by high spatiotemporal correlations in recurrent networks (Daucé et al. (2002); Yoshioka et al. (2007)). Although this correlated activity has been experimentally observed in many brain regions during memory-related tasks, including hippocampal CA3 (O'Keefe and Recce (1993); Traub et al. (1989)), it remains unknown how correlations regulate and organize the memory within recurrent networks at synaptic level.

In this paper, we first investigate the mechanism whereby STDP can lead to reliable storage and retrieval of simple synaptic patterns within a generic self-organized recurrent network. We then show how spatiotemporal correlated activity influences simple pattern formation and completion. We demonstrate that the storage process does not *require*, but is *accelerated* by spatially correlated firing among both layers of cells. However, we find that at the "recall" stage, transferring the stored recurrent pattern into the feedforward synapses of a reconstruction layer *does* require the presence of spatially correlated background activity. We then explore the relationship of learning curves and the time constants of correlated activity. Finally, we analyze the memory capacity of a recurrent network under assumptions of differing network size and connection probability. Our model is consistent with the reported literature on both "hard-bound" and "soft-bound" of STDP dynamics. These results suggest a possible generic mechanism of cortical memory organization and retrieval by STDP in self-organized recurrent networks.

2 MATERIAL & METHODS

2.1 Neuron models

To investigate the synaptic dynamics, we simulated leaky integrate-and-fire neurons(LIF) as in Brette et al. (2007), where each neuron was described by a single-compartment model with a time constant, $\tau = 20\ ms$, a leaky conductance of $5\ nS$, and leak reversal potential, $E_L = -60\ mV$. These parameters corresponded to a $100\ pF$ capacitance. The subthreshold membrane potential obeyed the following equation:

$$\tau \frac{dV}{dt} = -(V - E_L) - \tilde{\omega}_{exc}\,(V - E_{exc}) - \tilde{\omega}_{inh}\,(V - E_{inh})\,. \tag{1}$$

Both excitatory and inhibitory synapses were simulated as conductance changes with instantaneous jump at maximal value and exponential decay according to the following equation:

$$\tilde{\omega}_{exc,inh}(t) = \omega_{exc,inh} \times e^{-t/\tau_{exc,inh}}\,, \tag{2}$$

where $\tau_{exc} = 5\ ms$ and $E_{exc} = 0\ mV$ for excitatory synapses, $\tau_{inh} = 10\ ms$, and $E_{inh} = -80\ mV$ for inhibitory synapses. All synapses had the same synaptic delay as $1\ ms$. In most situations, the quantal conductance was $5\ nS$ for both feedforward and background excitatory connections, $1\ nS$ for recurrent excitatory connections, and $50\ nS$ for inhibitory connections, unless specified. The time step of the integration is $0.1\ ms$ in all simulations. We also performed the simulation with shorter time step, and there is no qualitative changes in the results.

2.2 Network model

The network was composed of three layers of neurons: a training layer (T), a recurrent layer (R) and a reconstruction layer (C), where each layer contained 100 neurons. Both T and C layers maintained all-to-all feedforward excitatory connections to the R layer with $\overline{\omega}_{\text{train}}$ = $\overline{\omega}_{\text{recon}}$ = $5\ nS$, while R contained local excitatory connections at $\overline{\omega}_{\text{recurr}}$ = $1\ nS$ with connection probability of $\rho = 100\%$, unless specified. In general, we denote the $\overline{\omega}$ as the upper bound of synaptic weights subject to STDP, and ω as the modulated maximal conductance in Equ. 2. In addition, each neuron of R also received a single excitatory background input E (corresponding to 100 one-to-one connections) and 25 inhibitory independent inputs (pool of 2500 neurons), where both types maintain fixed maximal conductances according to Equ. 2. We chose a 4:1 ratio of feedforward excitatory to inhibitory connection to mimic a balanced state of network activity (van Vreeswijk and Sompolinsky (1996)). In sum, each neuron in R received synaptic current from four sources at the same time, as following:

$$I_i^{recurr} \;=\; I_i^{bg} \;+\; \sum_{j=0, j\neq i}^{N_R=\rho N} I_i^{recurr} \;+\; \sum_{j=0}^{N_{T/C}=N} I_j^{train/recon} \;+\; \sum_{j=0}^{N_I} I_j^{inh}\ , \tag{3}$$

where $N = 100$ and $N_I = 25$. In the experimental scenario, either T or C was presented as an input (not both at the same time). The local recurrent excitatory connections in R, on one hand, and feedforward connections between C and R, on the other hand, were subject to STDP rule during learning and recall stage, respectively. The connection probability ρ and size of R were varied to estimate their impact on the pattern storage and reconstruction.

The feedforward layers, T and C, were simulated to reproduce an ongoing activity at $50\ Hz$, which was spatiotemporally correlated with the background activity in R. The single input of excitatory background activity I_i^{bg} (denoted as E) fired at a peak rate of $1000\ Hz$ to represent the large number of afferents on R. (see Sec. 2.3 for an explanation). The 25 inhibitory inputs I_j^{inh} were simulated as Poisson process at a fixed $10\ Hz$, whose role was to prevent R from over-firing.

During the training phase, feedforward connection strengths $\omega_{\text{ji}}^{\text{ff}}$ between T and R were set to the following template pattern:

$$\omega_{ji}^{ff} \;=\; \begin{cases} \overline{\omega}^{train}\ , & \text{if} \mid j-i \mid \bmod (100-d) \leq d \\ 0nS\ , & \text{if} \mid j-i \mid \bmod (100-d) > d \end{cases}\ . \tag{4}$$

Viewed as a square matrix of $N \times N$ binary connections (when $\rho = 1\%$), this template assumed the shape of a main diagonal of width $2d$, with periodic boundary conditions (creating two additional triangular corners of width d; see Fig. 3). Typically, we set $d = 20$ for $N = 100$. The upper bound value of synaptic weight was set to $\overline{\omega}_{\text{train}}$ = $5\ nS$. Network development proceeded in two phases (Fig. 1):

- During the training phase, the synaptic pattern of $T \xrightarrow[forward]{feed} R$ connections was clamped to ω_{ji}^{ff} according to Equ. 4, while the recurrent $R \rightarrow R$ synapses were allowed to develop according to the STDP rule. This represented a learning process in which sensory stimulus was applied to R to form a memory.
- During the reconstruction phase, another layer of $C \xrightarrow[forward]{feed} R$ connections was put in place and subjected to the STDP learning rule, while R's synaptic weights were maintained at their mature value created during the training phase. The results were the recovery of the same $T \xrightarrow[forward]{feed} R$ pattern used during training, *i.e.,* the $C \xrightarrow[forward]{feed} R$ connections converged to ω_{ji}^{ff}.

2.3 Spatiotemporally correlated ongoing activity

Ongoing activity is simply generated by correlating the background input E of recurrent layer R with either the training layer T or the reconstruction layer C. The neurons of T and C generated spikes following an inhomogeneous Poisson random process, in which the spatio-periodic firing rate of neuron i depends on the stimulus location s (Song and Abbott (2001)):

$$r_i \;=\; r_{max} \;\times\; (e^{-(s-i)/2\sigma^2} \;+\; e^{-(s-i+100)/2\sigma^2} \;+\; e^{-(s-i-100)/2\sigma^2}) \;, \tag{5}$$

where $r_{max} = 50\ Hz$ and $\sigma = 10$. According to Equ. 5, neurons exhibited maximal firing rate at location s (the last two terms are added to implement periodic boundaries in 1D space). To generate time-varying firing rates, we update r_i for each time interval, which was drawn from exponential distribution with mean $\tau_{\text{corr}} = 20\ ms$, unless specified. Here, we define the decay time constant of stimuli τ_{corr} as the temporal correlation constant. The background input of R (denoted E above) generated spikes through the same mechanism ($\sigma = 10$, $\tau_{\text{corr}} = 20\ ms$), except with $r_{max} = 1000\ Hz$ to mimic massive afferent activity.

Experiments show that neurons with higher instantaneous firing rate, are more likely to correlate with the spontaneous ongoing activity (Tsodyks et al. (1999)). In order to train and reconstruct the synaptic pattern at R layer, the spatial correlation was introduced between the background input of R layer and T/C layers according to the following equation:

$$s_{rc/ff} \;=\; s \;+\; (N + \sqrt{c} \times \;(1 \;-\; N)) \;\times\; g \;, \tag{6}$$

where c $(0 \leq c \leq 1)$ is the spatial correlation coefficient, $g \sim U[0,1]$ is standard uniform random number (Rudolph and Destexhe (2001); Zou and Destexhe (2007)). For every interval, a random location s was first generated from a uniform distributions between 0 and $N-1$ ($N = 100$). At the start of each interval, the stimulus location in feedforward T/C layer, s_{ff} and in recurrent R layers, s_{rc} were correlated at c through Equ. 6, then the firing rates of neurons in each layer were generated according Equ. 5 and held constantly until next interval. In this way, the neurons which had the maximal instantaneous firing rates in both R layer and T/C layer, shared the spatiotemporally correlated ongoing activity (Tsodyks et al. (1999)).

2.4 STDP models

The STDP mechanism we used in our simulation is similar to Song et al. (2000).

$$\frac{d\omega}{dt} \;=\; \Big[F_{LTP}(t) \;-\; F_{LTD}(t)\Big]_{\omega_{LTD}}^{\omega_{LTP}} \;, \tag{7}$$

where synaptic weight is bounded between $\omega_{\rm LTP}$ and $\omega_{\rm LTD}$. Therefore, the modulation of ω has "hard bounds". In contrast, we also consider a model with "soft bounds", where the changes of ω depend on the value of the weight (Zou and Destexhe (2007)):

$$\frac{d\omega}{dt} = F_{LTP}(t)(\omega_{LTP} - \omega) - F_{LTD}(t)(\omega - \omega_{LTD}) \ . \tag{8}$$

By default, $\omega_{\rm LTP}$ and $\omega_{\rm LTD}$ are set to $\overline{\omega}$ and 0, respectively in both models.

We use functions $\mathrm{F_{LTP}}(t)$ and $\mathrm{F_{LTD}}(t)$ to describe the coincidence between the pre- and post-synaptic spikes for both hard and soft bounds models:

$$\begin{aligned} F_{LTP} &= \sum_{t_j<t_i\leq t} P(t-t_j)\,\delta(t-t_i) \\ F_{LTD} &= \sum_{t\geq t_j>t_i} Q(t-t_i)\,\delta(t-t_j)\ , \end{aligned} \tag{9}$$

where t_j and t_i are the timing of pre- and post-synaptic spikes, respectively, $\delta(t)$ is Dirac delta function representing a spike at time t, and all possible pairs of pre- and post-synaptic spikes are integrated by the summation. $P(t) = A_p \exp(-t/\tau_p)$ and $Q(t) = A_q \exp[-|t|/\tau_q]$ define the time window of interaction between spikes ($\tau_{\rm p} = \tau_{\rm q} = 20\ ms$). For recurrent synapses, learning take $\mathrm{A_p} = 0.005$, and $\mathrm{A_q} = 0.00525$, which gives $\mathrm{A_q}\tau_{\rm q}/\mathrm{A_p}\tau_{\rm p} = 1.05$ in the range of model from Song et al. (2000). Between feedforward and recurrent synapses, $\mathrm{A_p} = 0.005$, and $\mathrm{A_q} = 0.0058$, which makes $\mathrm{A_q}\tau_{\rm q}/\mathrm{A_p}\tau_{\rm p} = 1.16$. In addition, longer time window in either LTP or LTD are tested together with longer correlation time constant for the model of Song *et al.* (2000).

2.5 Similarity of synaptic patterns

The output synaptic patterns of C layer were quantified by determining how similar the patterns were close to the initial synaptic patterns of T, which are constrained by Equ. 4. Although synaptic pattern of R developed in a self-organized way, interaction between decay time constant $\tau_{\rm corr}$ and STDP function swaps the off-diagonal and diagonal connection in recurrent network R (see Sec. 3.4). This dichotomy suggests that we could simply define the predicted recurrent pattern as the off-diagonal connection pattern for intial diagonal connection pattern in T:

$$\omega_{ji}^{rc} = \begin{cases} 0nS\ , & \mathrm{if}|\ j-i\ |\ \mathrm{mod}\ (100-d) \leq d \\ \overline{\omega}^{recurr}\ , & \mathrm{if}|\ j-i\ |\ \mathrm{mod}\ (100-d) > d \end{cases} \ . \tag{10}$$

To measure the magnitude of varying quantity, we take the *Root Mean Square* ($r.m.s$) between the observed synaptic weight and the estimated ones as following:

$$r.m.s_{error} = \sqrt{\frac{1}{M}\sum_{ji}(\omega_{ji}^{observe}/\overline{\omega}_{ji} - \omega_{ji}^{predict}/\overline{\omega}_{ji})^2}\ , \tag{11}$$

where $\omega_{\rm ji}^{\rm observe}$ represents the observed synaptic weight, $\omega_{\rm ji}^{\rm predict}$ represents the initial synaptic weight being trained, and M represents the total number of synapses. $\overline{\omega}_{\rm ji}$ is the maximal synaptic weight, which is either

$\overline{\omega}_{\text{recon}} = 5\ nS$ for feedforward synapses or $\overline{\omega}_{\text{recurr}} = 1\ ns$ for recurrent ones. Since we take the percentage of the synaptic weights in equation above, the final *r.m.s.* will vary between 0 and 1.

All simulations and analyses were performed by NeoCortical Simulator (NCS) implemented with LINUX MPI on a Beowulf cluster (Brette et al. (2007); Hoang et al. (2013)). NCS input code were generated by a Python tool kit BrainLab (Drewes et al. (2009)).

3 RESULTS

3.1 Synaptic pattern training

At training stage, we consider the synaptic pattern training in the recurrent network by taking the feedforward pattern of $d = 20$, with the maximal strengths at the periodic diagonal band. Both feedforward and recurrent layers were spatiotemporally correlated at $c = 0.8$ and$\tau_{\text{corr}} = 20\ ms$. After 20k seconds with STDP applied at recurrent synapses, the initial uniformly distributed synaptic weights developed the maximal strengths at the off-diagonal band, complementary to the feedforward pattern as shown in Fig. 2A (also see the Supplementary Video 1). The distribution of synaptic weights is bimodal in Fig. 2B, with most of the synaptic weights depressed (Song et al. (2000)). The average instantaneous firing rates of the recurrent layer were slightly decreased from $12.1\ Hz$ to $10.7\ Hz$ during the first and last 100 seconds, respectively during the training process, while the peak ISI stays unchanged (Fig. 2C).

The mechanism of off-diagonal band formed at the recurrent layer could be explained with respect to the distribution of spike pair time interval Δt in Fig. 4A. Each training neuron synapses 40 recurrent neurons according to Equ. 4, and training layer generates periodic peak firing neurons for index $s \pm 10$ under the correlation of 0.8, whenever a location s is chosen. Therefore, the recurrent neurons most likely will fire with correlation at least to their ± 10 recurrent local neighbor neurons, when the spiking training neuron was filtered by the fixed feedforward synaptic pattern. As a good indication of correlation, the time interval histogram of spike pairs in Fig. 4A shows that locally connected synapses on the diagonal band were slightly shifted with $-5\ ms < \Delta t < 0\ ms$, which gave overall depression when convolving with the negative-favored STDP learning; On the contrary, the post-pre synaptic time interval in Fig. 4A shows long-range connected synapses at off-diagonal band were slightly more correlated at $0\ ms < \Delta t < 5\ ms$. Because all connections have $1\ ms$ synaptic delay, there is a $1\ ms$ delay for the positive peak of spike timing correlogram in Fig. 4A, dash line. The delay is more noticeable in Fig. 4B, solid line. This implies that the coincidently spiking neurons will be depressed. Although the peak of positive correlation is small in Fig. 4A, dash line, the potentiation is sufficient enough to overcome the negative effect in the STDP learning rule and decorrelation due to synaptic delay, by carefully choosing the ratio of $\mathrm{A_q}\tau_{\mathrm{q}}/\mathrm{A_p}\tau_{\mathrm{p}}$ as 1.05.

To simplify the discussion, we identify a specific stimulus location as index 40 for a given time, the training layer elicited maximal firing at recurrent neuron index $30 \sim 50$ through the fixed synaptic pattern. These neurons will first fire spikes with correlation as in Fig.4A (solid line) through local synapses, *i.e.*, the diagonal region of index $30 \sim 50$. The spikes will then propagate to the rest of neuron through long-range synapses, *i.e.*, the off-diagonal region of $0 \sim 30$ and $50 \sim 100$, which will give more positive Δt count in Fig.4A (dash line).

3.2 Synaptic pattern reconstruction

At reconstruction stage, we consider the feedforward synaptic pattern between the reconstruction and recurrent layer by freezing the synaptic pattern formed at training stage. Here, we still take the same spatiotemporal correlation ($c = 0.8$, $\tau_{\text{corr}} = 20\ ms$) as the training stage. The initial uniformly distributed

feedforward synaptic weights recovered the maximal strengths at the diagonal band with 20k seconds plasticity applied as shown in Fig. 3A (also see the Supplementary Video 1). The distribution showed strong bimodal distribution as early as 10k seconds in Fig. 3B. The average instantaneous firing rate reduced from $7.9\ Hz$ to $5.8\ Hz$ of the first and last 100 seconds, respectively during reconstruction phase, with the peak ISI shifting to the left (Fig. 3C).

The reason that the reconstruction layer can recover the pattern trained at recurrent layer before is due to the spatiotemporally correlated on-going activity. If both reconstruction and recurrent layer are activated simultaneously at the same neuron index, the reconstruction layer will have the accurate spike-timing response from recurrent layer so that feedforward synapses can be recovered back to the original pattern. Fig. 4B. illustrates the spike pairs distribution between reconstruction and recurrent layers. The synapses located at diagonal region had a large peak with $0\ ms < \Delta t < 5\ ms$ (Fig. 4B, solid line), and was potentiated. Because of this large correlation peak, we could choose $\mathrm{A_q}\tau_\mathrm{q}/\mathrm{A_p}\tau_\mathrm{p}$ up to 1.16, but still develop the potentiated diagonal pattern. This could be understood as neurons without local connection responded more to pre-synaptic neurons. While synapses located along the off-diagonal region had a trough at $0\ ms < \Delta t < 5\ ms$ (Fig. 4B, dash line), which in turn depressed the synapses. This is due to the neurons with long-range connection firing spikes spontaneously and being reluctant to correlate with the pre-synaptic neurons. Although the spike pair counts at $|\Delta t| > 25\ ms$ are unbalanced (Fig. 4B), it has least impact on the overall effect when convolved with STDP modification function, because the largest modification happens at $|\Delta t| < 5\ ms$. The spatiotemporally correlated ongoing activity gave the reconstruction layer an exact reference of where the information is stored, and the asymmetric STDP rule shaped the synaptic pattern. As a control, we take a random recurrent pattern during reconstruction stage, and the resulting feedforward connection doesn't show any specific pattern, but rather synaptic competition as in Song et al. (2000) (figures not shown). This suggests that previously learned connectivity within R is necessary to reconstruct the feedforward connectivity.

To measure how well the synaptic patterns were trained and reconstructed, we calculated the root mean square (*r.m.s.*) between the actual synaptic map and the synaptic template defined as Equ. 7. The synaptic weights were sampled at every second, and fitted to exponential function as: $E_{rms} \times (1 - e^{-t^2/\tau_{rms}})$, where E_{rms} is the converged root mean square, and τ_{rms} is the time constant for the *r.m.s.* to converge. The trained synaptic map was index-wisely compared with the template map. The recurrent *r.m.s.* were almost saturated at 39.48% after 20k seconds of training, while the reconstructed synaptic pattern had similar quality with $E_{rms} = 38.26\%$, although it took longer to saturate in Fig. 4C.

3.3 Effect of spatial correlation on pattern formation

We next investigated the effect of spatial correlation between feedforward layer T/C and recurrent layer R (see Sec. 2.2). The *r.m.s.* of the stable synaptic weights is calculated to estimate how the synaptic map was trained and reconstructed from the template pattern. The time constant of the *r.m.s.*, τ_rms is also estimated from the exponential function to predict how fast the synaptic map reaches its stable state. Fig. 5A indicates that *r.m.s.* decreases when the spatial correlation increases for both training and reconstruction. However, spatial correlation is NOT necessary to form the recurrent pattern during training: the quality of recurrent synaptic map does not change from $c = 0.0$ to $c = 0.6$ (Fig. 5A, circle line and Fig. 5C, upper row). This suggests that the emerging weight structure in recurrent network does not depend on spatial correlation, and is ensured by the temporal correlation $\tau_\mathrm{corr} = 20\ ms$ (see Sec. 3.4 for effect of temporal correlation). In contrast with the training, spatial correlation significantly changed the *r.m.s.* during reconstruction (Fig. 5A,

triangle line and Fig. 5C, bottom row). The pattern is not formed until $c = 0.6$. This suggests that STDP operates mainly via rate effects.

The time constant of *r.m.s.* during training $\tau_{\mathrm{rms}}^{\mathrm{train}}$ ranges from 144 to 220 seconds, and correlation monotonically decrease the time constant (Fig. 5B, circle line). By examining the scales of time units, we notice that the time constant for reconstruction is longer than the one of training by an order of magnitude. This result could be explained by the fact that fast learning usually is followed by more gradual improvements in memory (Alain et al. (2007)). However, the effect of the correlation on time constant of *r.m.s.* during reconstruction $\tau_{\mathrm{rms}}^{\mathrm{recon}}$ is rather complex: The synaptic map converged to stable value within 100 seconds without correlation introduced. $\tau_{\mathrm{rms}}^{\mathrm{recon}}$ jumped up to about 7700 seconds when correlation was first introduced, then start to decrease when reconstructed synaptic pattern emerged at $c = 0.6$ (Fig. 5C, bottom row).

3.4 Influence of decay time constant of stimuli and STDP function

During both training and reconstruction of synaptic pattern, both recurrent and feedforward networks receive input stimuli generated by a short period of burst presented at random locations. The decay time constant of the stimuli, *i.e.,* the time lasting before an input burst moves to another random location, was chosen from an exponential distribution with a mean of 20 ms in previous simulation. To investigate the influence of longer time constant of stimuli on the synaptic pattern formation, we increase the time constant of stimuli, τ_{corr}, from 20 to 100 ms (Fig. 6A). The increase of τ_{corr} strongly degrade the quality of the synaptic pattern formed in feedforward network (Fig. 6A, bottom middle), because of the disappearing of the potentiation peak in correlation (Fig. 6B, compare the dot dash line to solid line). However, longer τ_{corr} preserved the pattern formed in recurrent network (Fig. 6A, top middle), although *r.m.s.* has 3.84% increase and it takes about 10 times longer to stabilize the pattern compared to $\tau_{\mathrm{corr}} = 20\ ms$.

To further test the influence of time constant of the STDP function, we matched τ_{p} and τ_{q} with τ_{corr} during both training and reconstruction processes, respectively. We found that the formation of the pattern were improved, if τ_{p} matches τ_{corr} during training (Fig. 6A, top left) and τ_{q} matches τ_{corr} during reconstruction (Fig. 6A bottom right). The potentiation peak in the correlation (Fig. 6B) is responsible for the improvement of quality of the pattern during reconstruction (figure not shown during training). Interestingly, the synaptic patterns were swapped, if τ_{q} matches τ_{corr} during training (Fig. 6, top right) and τ_{p} matches τ_{corr} during reconstruction (Fig. 6, bottom left). Both diagonal and off-diagonal connection patterns in recurrent network during training (Fig. 6A, upper row) shows that strong synapses are bidirectional. The relatively larger peak at positive intervals in Fig. 6C contributes to the dominance of the potentiation at the swapped region of the pattern during reconstruction (figure not shown during training).

4 DISCUSSION

We presented a novel model wherein simple synaptic patterns are stored into and retrieved from a recurrent network through STDP under conditions of correlated spatiotemporal activity. As signals, we used very general Poisson spike trains with a Gaussian distribution of firing rates (Song et al. (2000)) , with correlation centered at the peak firing frequency. Connectivity patterns in a recurrent cortical network have been shown to be nonrandom (Song et al. (2005)). Here we limit the pattern to simple diagonal connectivity, *i.e.,* short-range synapses, suggest a role for STDP to selectively potentiate synaptic patterns (Zou and Destexhe (2007)), and promote resonant learning in recurrent networks (Daucé et al. (2002)).

Our model could be applied generically to spiking networks that must transfer, store, then re-transfer simple synaptic patterns into another network. The paradigm might serve the underlying biological mechanism for the reward based system of Krichmar and Röhrbein (2013) or virtual neurorobotics (VNR) environment of Goodman et al. (2007). This is relevant in context of brain areas that have been shown to demonstrate both STDP and correlated spatiotemporal activity. The model provides a microcircuit-level explanation of how correlated activity temporally conjoins neurons into assemblies and selectively facilitates synaptic plasticity to support information storage and retrieval. For example, this been observed in hippocampus, especially CA3 (O'Keefe and Recce (1993); Traub et al. (1989)), which is known for its prominent recurrent synapses. Functionally, synaptic modification in hippocampus during task performance (such as navigation) is compatible with the dynamical organization and computational concept of our model. Likewise, correlated neuronal activity in neocortex has been observed while learning sensory input (Laurent and Davidowitz (1994); Linkenkaer-Hansen et al. (2001); Tateno et al. (2005); Pillow et al. (2008)), retrieving sensorimotor associations (Abeles et al. (1993); Vaadia et al. (1995)), and making decisions (Shadlen and Newsome (2001)). Cerebellar studies also show correlated spatiotemporal patterns (Middleton et al. (2008); Pillow et al. (2008)). A series of combined electroencephalogram (EEG) and intracellular *in vivo* measurements suggested that the required spatiotemporal correlation can arise from synchronous oscillation generated by the correlated activity of a population of neurons, during both awake and sleep states (Contreras and Steriade (1997); Destexhe et al. (1999); Buzsáki and Draguhn (2004)).

In this work, we define the temporal correlation constant, τ_{corr}, as the mean of the update time intervals for inhomogeneous Poisson process, and study the relationship between τ_{corr} and STDP learning time constant (either τ_{p} or τ_{q}). This temporal correlation mechanism represents global discontinuity for saccades in vision and sniff in olfaction (Uchida et al. (2006)), or brain oscillation (Contreras and Steriade (1997); Destexhe et al. (1999); Buzsáki and Draguhn (2004)). This contrasts with previous works that temporal sequences were presented continuously where afferents fire continuously with a constant population rate (Masquelier et al. (2008); Nowotny et al. (2003)).

How sensitive are the parameters of STDP to achieve learning and recall in our model? We first explored the effect of changing the background temporal correlation time constant, τ_{corr}, on pattern formation during each of the phases. Surprisingly, storage of the feedforward to recurrent synaptic pattern was minimally affected by increasing τ_{corr} alone, in the physiological range of 20 to 100 ms (Fig. 6A, top left). Increasing τ_{corr} in concert with an increase of the positive learning time constant, τ_{p} as high as 100 ms enhances the efficiency of initial pattern storage of into the recurrent network (Fig. 6A, top middle). In either case, the synaptic patterns have formed a long-range bidirectional connection. Although such a large τ_{p} has not yet been reported, it is believed that such a widened LTP window can result from NMDA channel activation or calcium diffusion (Badoual et al. (2006)). On the other hand, increasing τ_{corr} alone will impair the recalled pattern (as reported also by Song and Abbott (2001)); however, we found that this impairment is alleviated if the negative learning time constant, τ_{q}, is concurrently increased to 100 ms (which also results in an inversion of the stored pattern of synaptic strengths in both recurrent and feedforward networks). Prolongation of τ_{q} on this scale has been reported in rats (Feldman (2000)) and electric fishes (Bell et al. (1997)). In this case, a short-range bidirectional connection has been formed in the recurrent network. Nevertheless, Both long- and short-range bidirectional connections are potentiated (Song et al. (2005)).

We also evaluated the impact of imposing "soft-bound" STDP rules (Kistler and van Hemmen (2000); van Rossum et al. (2000); Badoual et al. (2006); Morrison et al. (2007); Zou and Destexhe (2007)). We found that "soft-bound" STDP results in the formation of synaptic patterns at about the same rate as does the "hard-bound" model, but it produces a low contrast pattern, attributable to the unimodal distribution

of the synaptic weights. Thus our spatiotemporal correlation–based computing paradigm of synaptic pattern storage and retrieval is independent from whether "soft-" or "hard-bound" rule is applied. The effects of the recurrent network size and connectivity are investigated by performing the pattern training and reconstruction as well. Interestingly, all simple recurrent patterns, although at different levels of connectivity and size, contain essential information to reconstruct the feedforward patterns initially trained.

The accuracy of pattern storage of our model was also evaluated using root mean square ($r.m.s$) error while co-varying the connectivity and size of the recurrent network. In general, a sparsely connected but larger size recurrent network (for example, 20% with 100 neurons) will have better performance on pattern storage and retrieval. We did not study recurrent networks larger than 100 neurons, due to the computational overhead involved. Further work should also include the evaluation of clustering of complex synaptic patterns under different conditions of brain activity.

DISCLOSURE/CONFLICT-OF-INTEREST STATEMENT

The authors declare that the research was conducted in the absence of any commercial or financial relationships that could be construed as a potential conflict of interest.

ACKNOWLEDGMENTS

In memory of Dr. Philip H. Goodman.

SUPPLEMENTAL MATERIAL

The Supplementary Information, Supplementary Videos 1 and 2 for this article can be found at http://www.cse.unr.edu/brain/.

REFERENCES

Abeles, M., Bergman, H., Margalit, E., and Vaadia, E. (1993). Spatiotemporal firing patterns in the frontal cortex of behaving monkeys. *J Neurophysiol* 70, 1629–1638

Alain, C., Snyder, J. S., He, Y., and Reinke, K. S. (2007). Changes in auditory cortex parallel rapid perceptual learning. *Cerebral Cortex* 17, 1074–1084

Badoual, M., Zou, Q., Davison, A. P., Rudolph, M., Bal, T., Frégnac, Y., et al. (2006). Biophycial and phenomenological models of multiple spike interactions in spike-timing dependent plasticity. *Int J Neural Systems* 16, 1–19

Bell, C. C., Han, V. Z., Sugawara, Y., and Grant, K. (1997). Synaptic plasticity in a cerebellum-like structure depends on temporal order. *Nature* 387, 278–281

Bi, G. Q. and Poo, M. M. (1998). Synaptic modifications in cultured hippocampal neurons: dependence on spike timing, synaptic strength and postsynaptic cell type. *J Neurosci* 18, 10464–10472

Brette, R., Rudolph, M., Carnevale, T., Hines, M., Beeman, D., Bower, J. M., et al. (2007). Simulation of networks of spiking neurons: A review of tools and strategies. *J Comput Neurosci* 23, 349–398

Buzsáki, G. and Draguhn, A. (2004). Neuronal oscillations in cortical networks. *Science* 304, 1926–1929

Contreras, D. and Steriade, M. (1997). Synchronization of low-frequency rhythms in corticothalamic networks. *Neurosci* 76, 11–24

Daucé, E., Quoy, M., and Doyon, B. (2002). Resonant spatiotemporal learning in large random recurrent networks. *Biol Cybern* 87, 185–198

Davison, A. P. and Frégnac, Y. (2006). Learning cross-modal spatial transformations through spike timing-dependent plasticity. *J Neurosci* 26, 5604–5615

Destexhe, A., Contreras, D., and Steriade, M. (1999). Cortically-induced coherence of a thalamic-generated oscillation. *Neurosci* 92, 427–443

Drewes, R., Zou, Q., and Goodman, P. H. (2009). Brainlab: a python toolkit to aid in the design, simulation, and analysis of spiking neural networks. *Frontiers in Neuroinformatics* 3, 16

Feldman, D. E. (2000). Timing-based ltp and ltd at vertical inputs to layer II/III pyramidal cells in rat barrel cortex. *Neuron* 27, 45–56

Goodman, P. H., Buntha, S., Zou, Q., and Dascalu, S.-M. (2007). Virtual neurorobotics (vnr) to accelerate development of plausible neuromorphic brain architectures. *Frontiers in Neurorobotics* 1. doi:10.3389/neuro.12.001.2007

Hoang, R. V., Tanna, D., Jayet Bray, L. C., Dascalu, S. M., and Harris, F. C. (2013). A novel cpu/gpu simulation environment for large-scale biologically-realistic neural modeling. *Frontiers in Neuroinformatics* 7. doi:10.3389/fninf.2013.00019

Kistler, W. M. and van Hemmen, J. L. (2000). Modeling synaptic plasticity in conjunction with the timing of pre- and post-synaptic action potentials. *Neural Comp* 12, 385–405

Kitano, K., Câteau, H., and Fukai, T. (2002). Self-organization of memory activity through spike-timing-dependent plasticity. *NeuroReport* 13, 795–798

Krichmar, J. L. and Röhrbein, F. (2013). Value and reward based learning in neurorobots. *Frontiers in Neurorobotics* 7. doi:10.3389/fnbot.2013.00013

Laurent, G. and Davidowitz, H. (1994). Encoding of olfactory information with oscillating neural assemblies. *Science* 265, 1872–1875

Linkenkaer-Hansen, K., Nikouline, V. V., Palva, J. M., and Ilmoniemi, R. J. (2001). Long-range temporal correlations and scaling behavior in human brain oscillations. *J Neurosci* 21, 1370–1377

Magee, J. C. and Johnston, D. A. (1997). A synaptically controlled, associative signal for hebbian plasticity in hippocampal neurons. *Science* 275, 209–213

Markram, H., Lübke, J., Frotscher, M., and Sakmann, B. (1997). Regulation of synaptic efficacy by coincidence of postsynaptic APs and EPSPs. *Science* 275, 213–215

Masquelier, T., Guyonneau, R., and Thorpe, S. J. (2008). Spike timing dependent plasticity finds the start of repeating patterns in continuous spike trains. *PLoS One* 3, e1377

Middleton, S. J., Racca, C., Cunningham, M. O., Traub, R. D., Monyer, H., Knöpfel, T., et al. (2008). High-frequency network oscillations in cerebellar cortex. *Neuron* 58, 763–774

Morrison, A., Aertsen, A., and Diesmann, M. (2007). Spike-timing-dependent plasticity in balanced random networks. *Neural Comp* 19, 1437–1467

Nowotny, T., Rabinovich, M. I., and Abarbanel, H. D. I. (2003). Spatial representation of temporal information through spike-timing-dependent plasticity. *Phys Rev E* 68, 011908

O'Keefe, J. and Recce, M. (1993). Phase relationship between hippocampal place units and the eeg theta rhythm. *Hippocampus* 3, 317–330

Pillow, J. W., Shlens, J., Paninski, L., Sher, A., Litke, A. M., Chichilnisky, E. J., et al. (2008). Spatio-temporal correlations and visual signalling in a complete neuronal population. *Nature* 454, 995–999

Rudolph, M. and Destexhe, A. (2001). Correlation detection and resonance in neural systems with distributed noise sources. *Phys Rev Lett* 86, 3662–3665

Shadlen, M. N. and Newsome, W. T. (2001). Neural basis of a perceptual decision in the parietal cortex (area LIP) of the rhesus monkey. *J Neurophysiol* 86, 1916–1936

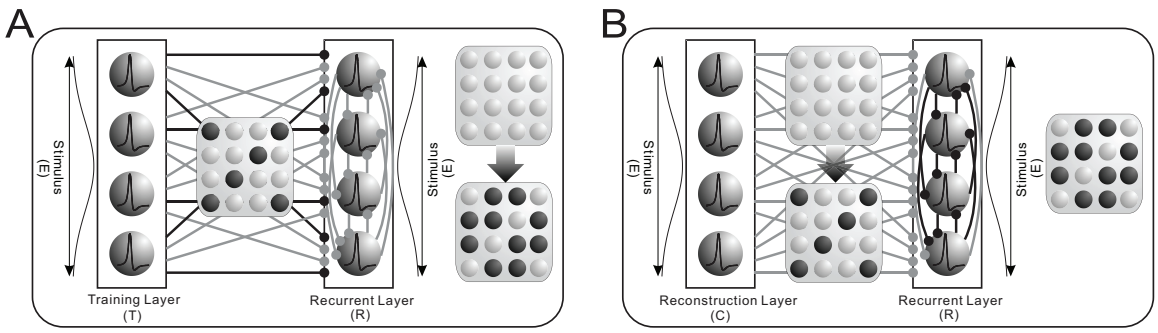

Figure 1. Training and reconstruction of synaptic patterns. (A) During training phase, The $T \rightarrow R$ synaptic pattern was fixed (diagonal matrix). The recurrent synaptic weights in R were subject to STDP rules and, starting from a uniform initial state, developed into an off-diagonal synaptic pattern. (B) During reconstruction phase, the recurrent synaptic pattern inside R was fixed, while $C \rightarrow R$ synapses were subject to STDP rules. Starting from a uniform distribution, the $C \rightarrow R$ synaptic weights reconstructed the diagonal pattern that was used during training in (A). Both T, R and C, R received spatiotemporally correlated background stimuli E in the 2 phases.

Song, S. and Abbott, L. F. (2001). Cortical development and remapping through spike timing-dependent plasticity. *Neuron* 32, 339–350

Song, S., Miller, K. D., and Abbott, L. F. (2000). Competitive Hebbian learning through spike-timing dependent synaptic plasticity. *Nature Neurosci* 3, 919–926

Song, S., Sjöström, P. J., Reigl, M., Nelson, S., and Chklovskii, D. B. (2005). The excitatory neuronal network of the c2 barrel column in mouse primary somatosensory cortex. *Neuron* 61, 301–416

Tateno, T., Jimbo, Y., and Robinson, H. P. (2005). Spatio-temporal cholinergic modulation in cultured networks of rat cortical neurons: evoked activity. *Neurosci* 134, 439–448

Traub, R. D., Miles, R., and Wong, R. K. S. (1989). Model of the origin of rhythmic population oscillation in the hippocampal slice. *Science* 243, 1319–1325

Tsodyks, M., Kenet, T., Grinvald, A., and Arieli, A. (1999). Linking spontaneous activity of single cortical neurons and the underlying functional architechture. *Science* 286, 1943–1946

Uchida, N., Kepecs, A., and Mainen, Z. (2006). Seeing at a glance, smelling in a whiff: rapid forms of perceptual decision making. *Nature Rev Neurosci* 7, 485–491

Vaadia, E., Haalman, I., Abeles, M., Bergman, H., Prut, Y., Slovin, H., et al. (1995). Dynamics of neuronal interactions in monkey cortex in relation to behavioural events. *Nature* 373, 515–518

van Rossum, M. C., Bi, G. Q., and Turrigiano, G. G. (2000). Stable Hebbian learning from spike timing-dependent plasticity. *J Neurosci* 20, 2211–2221

van Vreeswijk, C. and Sompolinsky, H. (1996). Chaos in neuronal networks with balanced excitatory and inhibitory activity. *Science* 274, 1724–1726

Yoshioka, M., Scarpetta, S., and Marinaro, M. (2007). Spatiotemporal learning in analog neural networks using spike-timing-dependent synaptic plasticity. *Phys Rev E* 75

Zou, Q. and Destexhe, A. (2007). Kinetic models of spike-timing dependent plasticity and their functional consequences in detecting correlations. *Biol Cybern* 97, 81–97

FIGURES

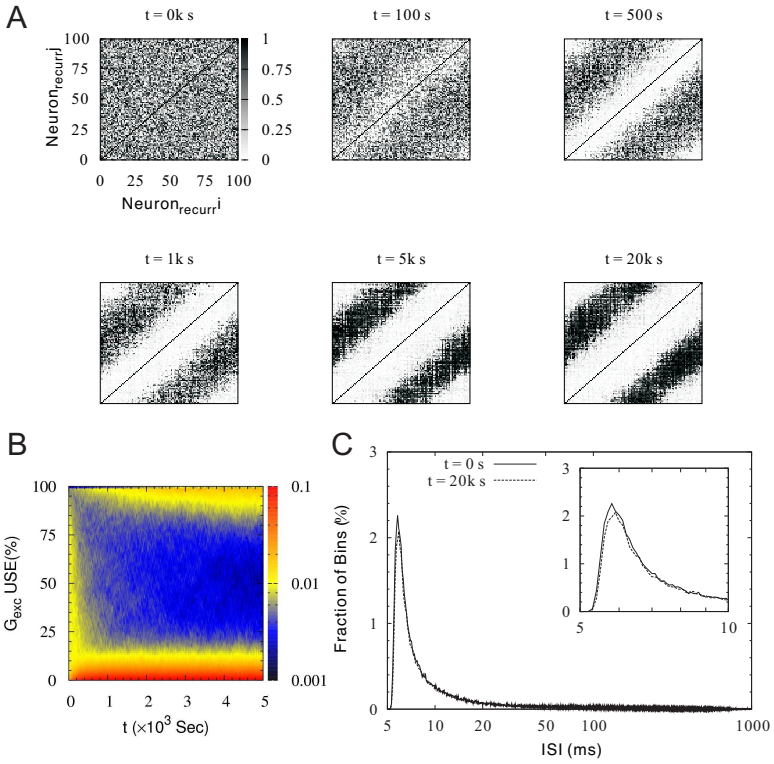

Figure 2. Training diagonal pattern at recurrent layer. (A) Snapshot of recurrent synaptic map was plotted at different time by averaging each synaptic strength over 10 seconds. Each pixel represents the synaptic strength from pre-synaptic neuron j to post-synaptic neuron i, which is normalized between 0 and 1 (see first snapshot for weight scale). All the synaptic weights are initialized uniformly. The synapses were selectively potentiated at the off-diagonal band, and depressed for the rest area during the training stage. The black pixel indicates self-connection which was excluded (see Supplementary Video 1). (B) Histogram of the synaptic weights plotted every 10 seconds over time. The bimodal distribution was formed at the end of training. (C) ISI distribution pooled from all the neurons of recurrent layer of 100 seconds duration shows no difference at start and end of the training, where both peak at 6$\sim$7 ms by noting the time is in log scale.

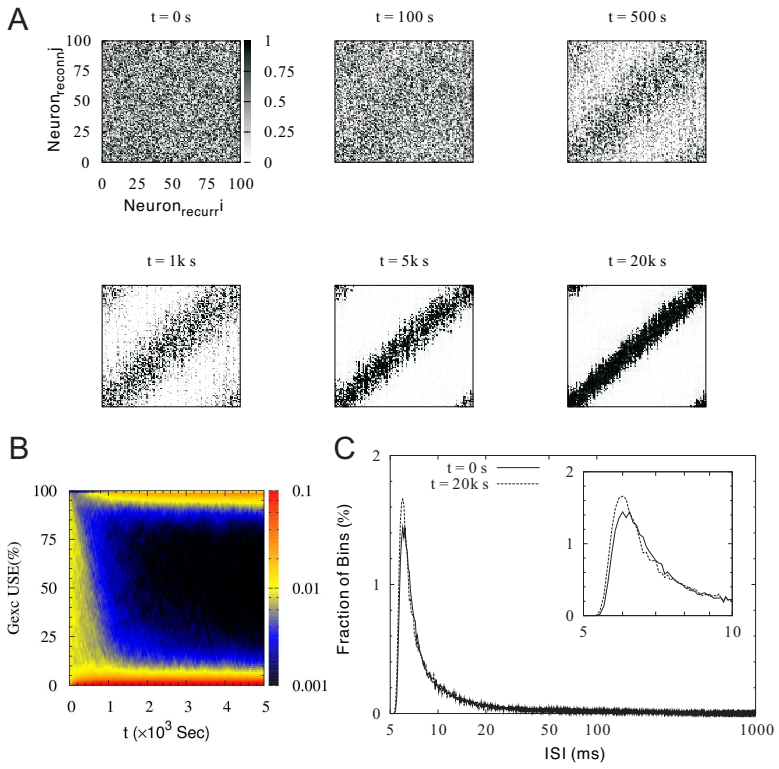

Figure 3. Rebuilding diagonal pattern at reconstruction layer. (A) Snapshot of feedforward synaptic map was plotted at different time by averaging each synaptic strength over 10 seconds. All the synaptic weights are initialized uniformly. The synapse map were exactly rebuilt as the periodic diagonal band which is trained at the recurrent layer before (see Supplementary Video 2). (B) Histogram of the synaptic weights plotted every 10 seconds over time. The strong bimodal distribution was formed at the end of training. (C) ISI distribution pooled from all the neurons of recurrent layer of 100 seconds duration shows the peak ISI was slightly shifted to the left after the reconstruction.

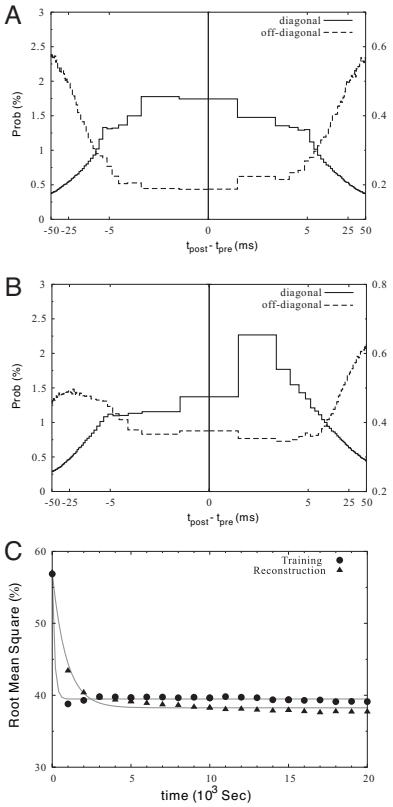

Figure 4. Spike pairs histogram and variances of synaptic patterns. All possible spike pairs $\Delta t = t_{post} - t_{pre}$ are binned for synapses both at diagonal band (solid line), and at off-diagonal band (dash line) with 1 ms time step after the synapses converged. The distribution were normalized to the total spike pair counts. Spike pair counts increase at small Δt for diagonal synapses, and decrease at small Δt for off-diagonal synapses. However, there are more counts for positive $|\Delta t| < 5$ ms at off-diagonal recurrent synapses (A), dot line and at diagonal feedforward synapses (B), solid line. In contrast, there are more counts for negative $|\Delta t| < 5$ ms at diagonal recurrent synapses (A), solid line and at off-diagonal feedforward synapses (B), dash line. The convolution of histogram with STDP function was evaluated to verify the weight drift (see text for details). (C) Root mean square (*r.m.s.*) of the varying magnitude between the estimated synaptic weights and the observed ones were measured every second (only plot with every 1000 seconds). The *r.m.s.* were fitted to exponential functions. The recurrent synaptic pattern (filled circle) has $E_{rms} = 39.48\%$, $\tau_{rms} = 144.4$ s; the reconstruction synaptic pattern (filled triangle) has $E_{rms} = 38.26\%$, $\tau_{rms} = 900.6$ s.

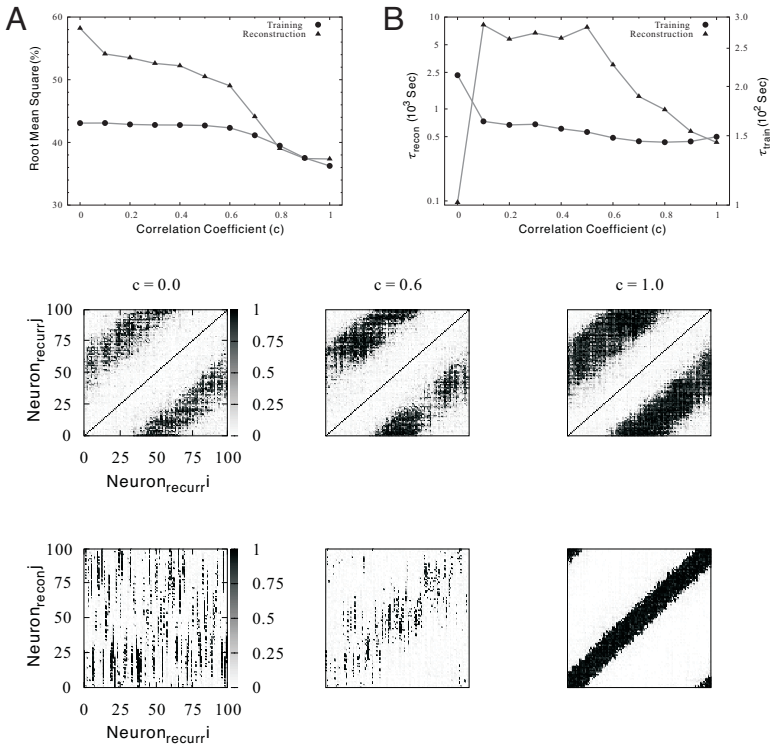

Figure 5. Effect of correlation on the $r.m.s_{\text{error}}$ and τ_{rms}. (A) Effect of correlation on the converged *r.m.s.* of training template pattern (filled circle) and reconstruction of the trained pattern (filled triangle). (B) Corresponding time constants were estimated by fitting *r.m.s.* to exponential function, and then plotted as a function of correlation. The time constant for reconstruction is longer than the one of training on an order of magnitude by noting the different scales. (C) Synaptic map of both training (top row) and reconstruction (bottom row) were plotted at 20k seconds for correlation being 0.0, 0.6 and 1.0.

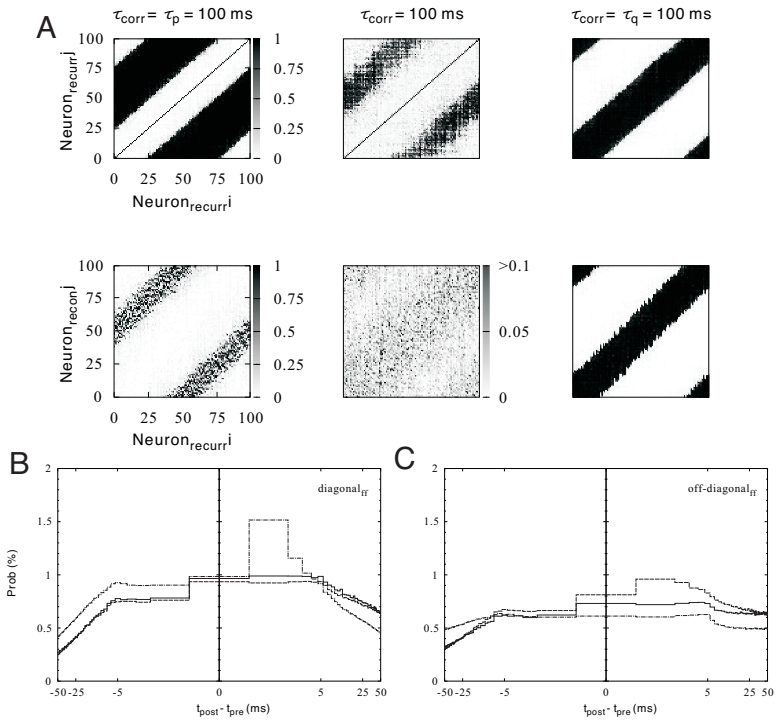

Figure 6. Effect of decay time constant of stimuli and STDP window function. (A) Both recurrent (top) and feedforward network (bottom) were undergone stimuli with correlation time, τ_{corr}, at 100 ms. Feedforward network had a degradation of the reconstructed synaptic pattern by noting the scale of the conductance (bottom middle), while recurrent network was not affected (top middle). The synaptic pattern can be preserved by matching τ_{corr} with τ_p during training (top left) and τ_q during reconstruction (bottom right), respectively. However, the synaptic patterns were swapped if $\tau_q = \tau_{corr}$ during recurrent training(top right), and $\tau_p = \tau_{corr}$ during feedforward reconstruction(bottom left). The correlation of the stimuli was 0.8 for all the simulations. Histogram of time interval, $t_{post} - t_{pre}$, for $\tau_{corr} = \tau_p = 100\ ms$ (dash), $\tau_{corr} = 100\ ms$ (solid) and $\tau_{corr} = \tau_q = 100\ ms$ (dot dash) at diagonal region (B), and off-diagonal region (C) was sampled during reconstruction shown at A bottom. There are peaks appearing at positive time interval for each region, which are responsible for the synaptic pattern formed with potentiated synaptic weights.